J. Appl. Comput. Mech., 8(4) (2022) 1387-1397
DOI: 10.22055/jacm.2022.40206.3537

ISSN: 2383-4536
jacm.scu.ac.ir

Shahid Chamran University of Ahvaz

Journal of Applied and Computational Mechanics

Research Paper

Studying the Strengthening Effect of Railway Ballast in the Direct Shear Test due to Insertion of Middle-size Ballast Particles

Jianxing Liu[1,2,3], Mykola Sysyn[3], Zhiye Liu[1,2], Lei Kou[3], Ping Wang[1,2]

[1] MOE Key Laboratory of High-speed Railway Engineering, Southwest Jiaotong University, Chengdu 610031, China, Email: jianxingliu@my.swjtu.edu.cn (J.L.)

[2] School of Civil Engineering, Southwest Jiaotong University, Chengdu 610031, China, Email: zhiyeliu@my.swjtu.edu.cn (Z.L.); wping@home.swjtu.edu.cn (P.W.)

[3] Department of Planning and Design of Railway Infrastructure, Institute of Railway Systems and Public Transport, Technical University of Dresden, 01069 Dresden, Germany, Email: mykola.sysyn@tu-dresden.de (M.S.); lei.kou@tu-dresden.de (L.K.)

Received March 04 2022; Revised April 14 2022; Accepted for publication April 26 2022.
Corresponding author: M. Sysyn (mykola.sysyn@tu-dresden.de)

Abstract: This paper summarized some common grading curves of ballast layers and found that the content of 16-32 mm ballast particles ("middle-size particles" in this paper) had a significant effect on the direct shear performance of the ballast layer. In this paper, the direct shear tests of the ballast layers with different contents of middle-size particles were reproduced using the discrete element method (DEM). Two different compactions of the ballast samples were used, and the reasons for the changes of shear strength of the ballast layers with different size distributions were analyzed from macroscopic and microscopic perspectives. The results showed that the strengthening effect of the ballast due insertion of middle-particles could only be observed for normally compacted ballast, whereas the same insertion with fully compacted ballast would decrease the shear strengths properties. The fully compacted ballast is subjected to the dilation. The reason of the strengthening effect for the normally compacted ballast were the contraction and dilation processes. Insertion of the middle-size particles up to 20-30% at most increase the dilation processes. Thus, the results show that the ballast layers with conventional narrow particle size distribution (narrow PSD) have higher shear strength than wide range particle size distribution (wide range PSD) if the ballast is good fully compacted. Additionally, it should be noted that the number of small particles will increase during the lifecycle of the ballast layer due to corner brakeage and the external contamination. Moreover, the drainage aspects of the wide range PSD should be considered. Therefore, the excessive insertion of middle-size particles is not justified.

Keywords: Railway; fines-free ballast; particle size distribution; direct shear test; discrete element method.

1. Introduction

A railway ballasted track mainly consists of steel rails, fastener systems, sleepers, ballast beds and subgrades, which is widely used in the worldwide railway constructions because of its good resilience, capacity of seepage and drainage, possibility of large adjustment and low cost [1, 2]. Gravel ballasts are processed from mountain rocks, and are piled up according to certain size distributions to form ballast beds, which provides performance of force bearing, force transmission and stability for railway ballasted track structures [3, 4]. The trains, temperature and other factors will produce vertical and horizontal forces on a track structure, and the adverse effects caused by these forces are mainly resisted by a ballast bed [5-7]. Harmful loads (e.g., compression, shear, vibration) will not only cause the crushing and breakage of ballast particles [8, 9], but also lead to the movement and rotation of ballast particles [10, 11], thus changing the internal structure of the ballast bed, resulting in reduction of the ballast bed resistance and stability, which seriously affects the traffic safety of railway [12, 13]. The shear strength of ballast layer plays an important role in the stability of ballast bed, especially the deformation of ballast bed under the longitudinal and lateral forces [14, 15].

The direct shear test of granular aggregates is one of the most basic methods to study the shear performance and bearing capacity of aggregates, which is widely used in geotechnical engineering. In order to clarify the shear strength of ballast bed and optimize the service performance of railway ballasted track, researchers and engineers carried out a large number of experimental studies and simulation analysis. Dowbrow et al. [16], Wnek et al. [17], and Indraratna et al. [18] used 300 mm × 300 mm direct shear boxes to conduct direct shear tests on dirty ballast aggregates. It was found that there were an obvious cohesive force (15-125 kPa) and a friction angle (38-53°) in dirty ballast aggregates. Danesh et al. also used a 300 × 300 mm direct shear box to study the effect of ballast degradation on the shear strength. The results showed that the shear strength decreased by 48% with the increase of degradation degree. The expansion angle of degraded ballast decreased with the increase of crushing ratio and normal stress. TolouKian et al. [19] conducted laboratory tests on clean and sand-contaminated ballast aggregates using a 440 × 360 mm direct shear machine. It was found that sand pollution reduced the shear strength and angle of effective shear resistance

Published online: May 08 2022

of ballast, and the critical percentage of ballast pollution was given. Jia et al. [20] analyzed the direct shear performance of the mixtures of cleaned deteriorated ballast (i.e., recycled ballast) and new ballast by laboratory tests and discrete element numerical simulations. The results showed that when the content of recycled ballast was less than 30 %, the shear strength of the mixture was not significantly reduced. Then the shear strength and coordination number decreased with the content of recycled ballast increased. On the other hand, some researchers believed that the dry ballast aggregates, even containing small particles, should not appear obvious cohesive force. The reason for the cohesive force was that the direct shear box was too small to simulate the real mechanical state of ballast aggregates [21, 22]. Stark et al. [21] developed a full-size direct shear box that can accommodate a sample about 1 m wide and 0.6 m deep. Estaire and Santana [22] carried out the direct shear tests of ballast in a large direct shear box with a shear plane of 1 m × 1 m and a thickness of 0.8 m. The large sample size made the shear behavior and shear strength parameters significantly different from the References [16-18], which was closer to the true direct shear performance of ballast. However, it is undeniable that despite the boundary effect caused by the box scales, the variation laws between the shear performance and the loading of ballast layer are similar [23]. In addition to paying attention to the relationship between the gradation and the shear strength (stability) of the ballast layer, researchers also try to improve the shear strength of the ballast layer by adding special materials such as geogrid and asphalt in the ballast layer. Alsirawan [24] discussed the role of geogrid in improving the load efficiency and reducing the settlement of common granular layers and compared many design methods with 3D finite element methods (FEM). Habashneh [25] and Ahmad [26] analyzed and evaluated the special reinforcement technologies of ballast layers. The results show that geogrid can effectively improve the strength and resistance of ballast layer, then the geosynthetics were suggested being used for the reinforcement of railway substructure. Qatamin et al. [27] discussed the application, function, design requirements and international experience of asphalt layer in railway ballast, and he found that the asphalt layer could improve the overall performance and the dynamical performance of a ballast bed. In addition, the PSD also affects the damping of a ballast layer. Kuchak et al. [28] improved the damper model to obtain a higher value of Modal Assurance Criterion (MAC) and a lower frequency deviation. Kuchak et al. [29] established an experimental model and an accurate FEM model of the track damping system. The developed FEM model was used to evaluate the efficiency of different damping parameters and damping vibrations.

It cannot be ignored that even ballast without fine particles, a slight change of the size distribution will also affect the mechanical properties of the ballast layer. That is why researchers and engineers set standards to limit the size distribution of ballast particles in ballast beds [30, 31] (See Fig. 1). An ideal gradation is usually considered to provide maximum density, so it can provide maximum contact between particles. Based on that concept, Fuller and Thompson [32] proposed an equation of maximum density gradation called 'Talbot Equation'. Roberts et al. [33] proposed a maximum density equation of power function n^{th} (th was usually 0.45), as shown in Equation (1):

$$P = 100(d / D)^{0.45} \tag{1}$$

where P is the percentage passing weight, d is the size of aggregate, and D is the maximum aggregate size.

However, the maximum density will lead to a serious decrease in the drainage capacity of ballast bed. Therefore, the gradation of ballast bed needs to be adjusted properly on the basis of ensuring the density of ballast bed. As shown in Figure 2, the common gradations listed in the American Railway Engineering and Maintenance-of-Way Association (AREMA) is AREMA No.3, AREMA No.4, and AREMA No.24 [34, 35]. The common ballast size distribution curves in Australia are Rail Infrastructure Corporation (RIC) and Queensland standards [36, 37]. The ballast size distribution curve used in France is 'FRENCH' in Figure 2 [38]. In addition, similar gradation ranges have been adopted in China and Germany [39, 40]. Profaner [41] pointed out that the optimal shear strength of ballast layer could be increased by increasing the proportion of 15% of 16-32 mm ballast particles (standard ballast gradation of German), but the shear strength of ballast layer would be significantly lower than that of the initial gradation after the proportion exceeded the specific limit value. Interestingly, the curve with an increased percentage of 16-32 mm particles was similar to the curves of AREMA No. 3 and FRANCE. However, Profaner did not analyze the reasons for the above phenomenon in his study because of the limitation of the technical conditions at that time. In addition, although there have been many studies on the laboratory experiments and numerical simulations of the ballast direct shear ability, most of them were committed to explaining the influence of the intrusion of fine particles (crushed ballast, sands, coals, etc.) on the performance of ballast layers (e.g., References [16-20, 42]). The conclusion of those studies was consistent: the intrusion of fine particles reduced the shear strength of ballast layers, as fine particles filled the voids originally used for friction and interlocking between ballast particles. The 16-32 mm particles in a ballast layer belong to the middle-size particles, and the reason why such particles make the performance of a ballast layer change is obviously different from that of fine particles.

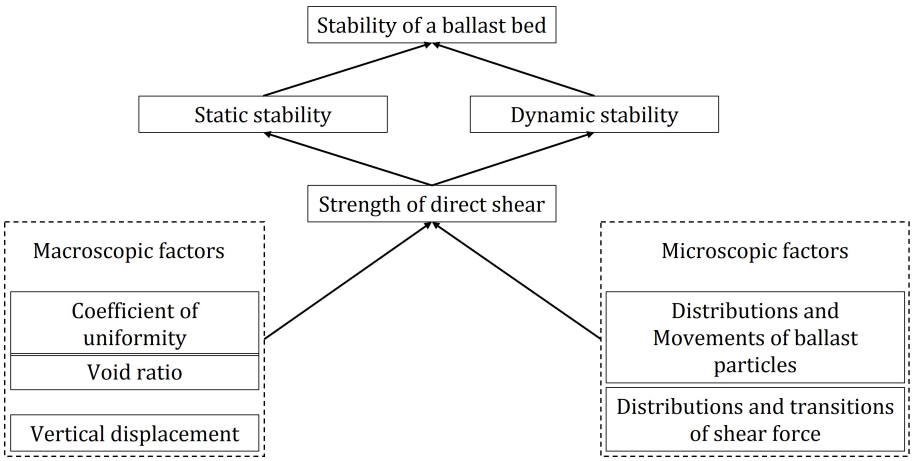

Fig. 1. Schematic configuration of the considered system.

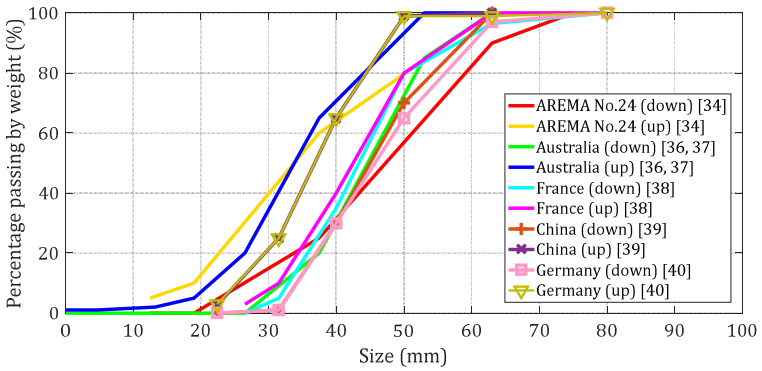

Fig. 2. Common particle size distributions (PSD) of ballast.

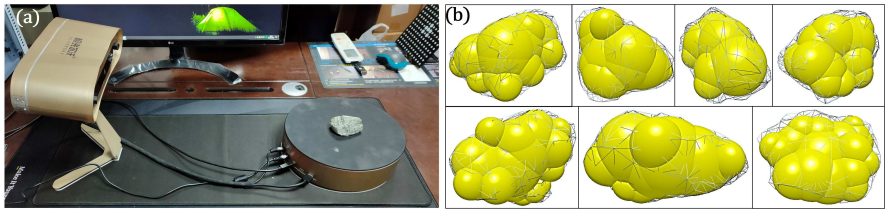

Fig. 3. (a) Ballast particle scanning, (b) 3D view of simulated particles.

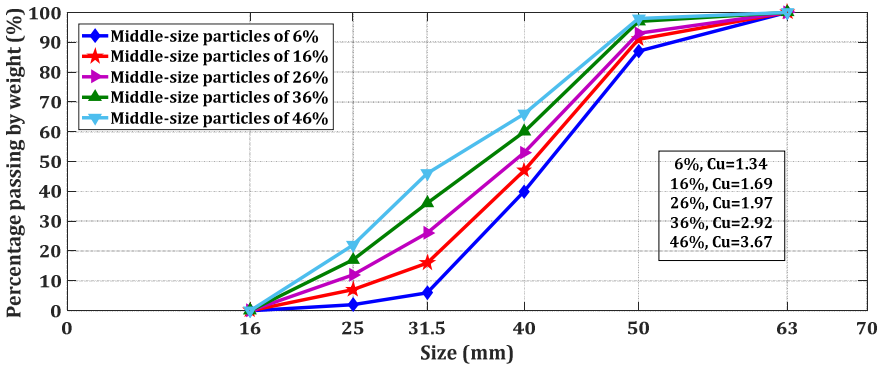

Fig. 4. PSD of the ballast samples.

The analysis of the present literature shows that effect of ballast strengthening for wide range PSD was presented in some studies [35]. However, the studies have not explained the intrinsic reasons of the phenomena in details and did not consider the additional factors influencing the effect. It is difficult to explore the state change of the particles in a ballast layer during direct shear tests through macroscopic physical experiments. The advantage of the discrete element method (DEM) is that it can simulate the movements of particles and help us understand the state change of particles from the mesoscopic perspective [43]. Therefore, the aim of this work is not only to reproduce the direct shear tests of ballast aggregates with different contents of middle-size particles by DEM, but also to analyze the reasons for the changes of shear strength of those ballast aggregates under the influence of fully compaction factor.

2. DEM Models and Loading Conditions

In order to clarify the meso-mechanical changes of the ballast aggregates with different contents of middle-size particles during direct shear tests, DEM was used to carry out the simulation analysis of the direct shear tests of ballast. The profiles of ballast particles were obtained by the 3D scanning technology, and they were filled by the clumped particle method [2], as shown in Figure 3.

The standard size distribution curve of ballast in the research work of Profaner [41] is the blue curve shown in Figure 4. We constructed a DEM direct shear model of ballast according to the standard ballast gradation, and its content of middle-size particles was 6% (mass percentage). Subsequently, according to Reference [41], the DEM models with the contents of middle-size particles exceeding 10%, 20%, 30% and 40% of the standard ballast gradation were established, that is, their contents of middle-size particles were 16%, 26%, 36% and 46%, as shown in Figure 4.

The size of upper shear box was 300 mm × 300 mm × 150 mm, and the size of lower shear box was 350 mm × 300 mm × 150 mm. It should be noted that the direct shear test of rock granular aggregates has the requirement for the size of direct shear box. The direct shear box used by Indraratna et al. [44] in the physical experiments and numerical simulations was 300 mm × 300 mm × 200 mm. Wang et al. [45] carried out the physical experiments and DEM simulations with a direct shear box of 300 mm × 360 mm × 240 mm. The upper direct shear box used by TolouKian et al. [46] was 440 mm × 440 mm × 180 mm, and the lower direct shear box was 540 mm × 440 mm × 180 mm. The authors comprehensively considered the shape and size of the direct shear box, and finally determined the shape and size of the direct shear box in this work combined with the actual situation in their laboratory. The material of boxes was steel. The area of both boxes was filled with ballast particles to achieve the same compactness as the samples in laboratory tests. In the next process, time was left to make the ballast aggregates stable. When everything was ready, a steel plate of 300 × 300 mm was applied to the top of the ballast models with a loading of 400 kPa for stable pressure. During the process of pressure stabilization, additional ballast particles were added to the space generated by

compression at the top of ballast layer, and the layer was compressed again. The above process was repeat until the ballast layer did not have significant compression. A horizontal loading of 32 kPa was applied to the lower shear box in stages until the displacement of the box reached 30 mm (10% of the length of the shear box). The five DEM direct shear models are shown in Figure 5 (a). Table 1-1 and Table 1-2 are the parameters of DEM models.

The models were initialized after the above 5 groups of calculations were completed. Then the coefficient of static friction and rolling friction of ballast-ballast were adjusted to 0 value, and the purpose is to make the ballast aggregates be sufficiently compacted under the compressive stress of 400 kPa. It should be noted that in order not to change the PSDs of ballast aggregates, no new particles were added. The parameters of ballast-ballast were restored to the value in Table 1, and a period of time was allowed for the ballast aggregates to stabilize after the ballast layers did not have significant compression (Figure 5 (b)). Finally, the direct shear tests were performed on the five new groups of ballast aggregates.

3. Results and Discussions

3.1 Comparison between the simulation results and previous studies

It can be seen from Figure 6 (a) that the direct shear curves of the five normally compacted ballast samples tend to be flat after the shear displacement exceeded 25 mm. In particular, the direct shear curve of the Content 46% is obviously flat when the displacement is 25 mm. It should be admitted that the DEM simulation results in this paper are not completely consistent with the experimental results of Reference [41]. DEM results show that the ballast aggregate with Content 36 % has the highest shear strength (the shear stress corresponding to the displacement of 30 mm is 504.25 kPa). The result in Reference [41] is that the ballast aggregate with Content 21% has the highest shear strength. That difference is mainly caused by the round surface of particles and the loss of friction between particles and walls. In addition, because the physical ballast particles were subjected to the vertical pressure and horizontal shear force in the direct shear tests, the breakage actually changed the content of middle-size particles in ballast aggregates [47-50]. Although the simulation values cannot be consistent with the experimental results in the previous research, the phenomenon that the direct shear strength of ballast changes with the content of middle-size particles does exist. That is, the shear strength of ballast increases first and then decreases with the increase of the content of middle-size particles. That phenomenon, that the existence of the optimal content of the middle-size particles in ballast layer, will significantly influence the bearing ability of ballast bed. On the other hand, the phenomenon that the direct shear strength of ballast changes with the content of middle-size particles is also presented in the fully compacted samples (Figure 6 (b)), but the distribution trends are different. The sample of Content 6% has a higher shear stress of 782.63 kPa at 30 mm than the rest samples. Thus, the strengthening effect of the ballast material due insertion of mid-particles can be only observed for normally compacted ballast, whereas such insertion with full compaction will decrease the shear strengths properties.

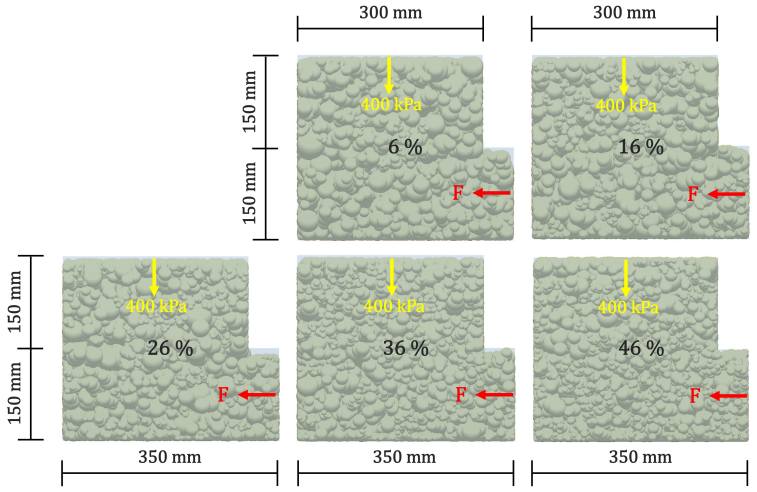

(a) Normally compacted samples

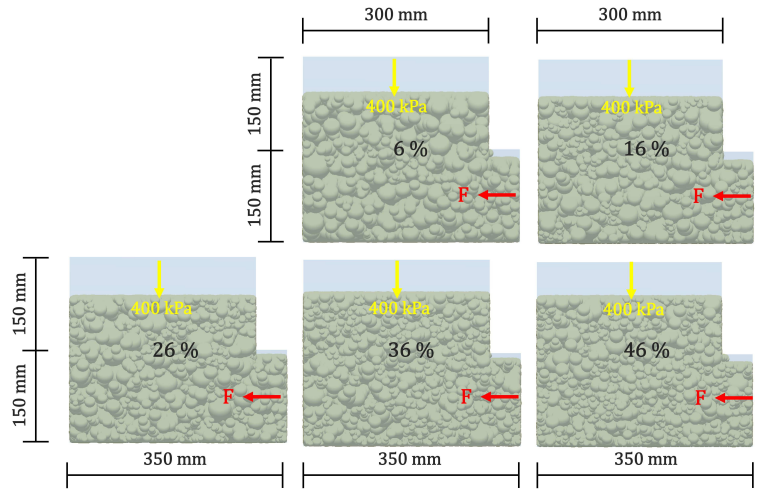

(b) Fully compacted samples

Fig. 5. DEM direct shear models with different contents of middle-size particles.

Table 1-1. Material parameters in DEM.

Poisson's ratio	Solid density	Young's Modulus
0.24	2660 kg/m^3	5×10^{10} Pa

Table 1-2. Contact parameters in DEM.

Types	Coefficient of restitution	Coefficient of static friction	Coefficient of rolling friction
Ballast-ballast	0.72	0.56	0.27
Steel-ballast	0.80	0.05	0.05

Table 2. Details of d60, d10 and C_u.

Contents	d_{60}	d_{10}	C_u
6%	44.23	33.01	1.34
16%	42.97	25.43	1.69
26%	41.78	21.21	1.97
36%	40.00	13.70	2.92
46%	37.46	10.21	3.67

3.2 Reasons for the influence of middle-size particles on the shear strength of ballast

This section comprehensively analyzes the reasons why the content of middle-size particles affects the shear strength of ballast from the perspectives. The analyzed factors include the coefficient of uniformity (C_u), void ratio, vertical displacement, particle movement and transitions of shear force.

3.2.1 Macroscopic factors

3.2.1.1 Coefficient of uniformity (C_u)

The coefficient of uniformity (C_u) is a factor used to evaluate the non-uniformity of particle size distribution in geotechnical engineering, as shown in Equation (2):

$$C_u = d_{60} / d_{10} \tag{2}$$

where d_{60} is the particle size whose total mass of particles is less than 60%, and d_{10} is the particle size whose total mass of particles is less than 10%. The details of d_{60}, d_{10} and C_u are listed in Table 2.

The relationship between the C_u values and shear strengths of the normally compacted and fully compacted samples is shown in Figure 6. It is obvious in Figure 7 that the increase of middle particles makes the C_u of ballast increase. The common experience suggests that the larger the C_u, the higher shear strength of granular aggregates [51]. However, the results show that when the C_u of ballast aggregate exceeds a certain limit (C_u = 2.55 for a normal ballast layer), the shear strength will be significantly reduced. In addition, the shear strength of fully compacted ballast aggregates decreases with the increasing C_u.

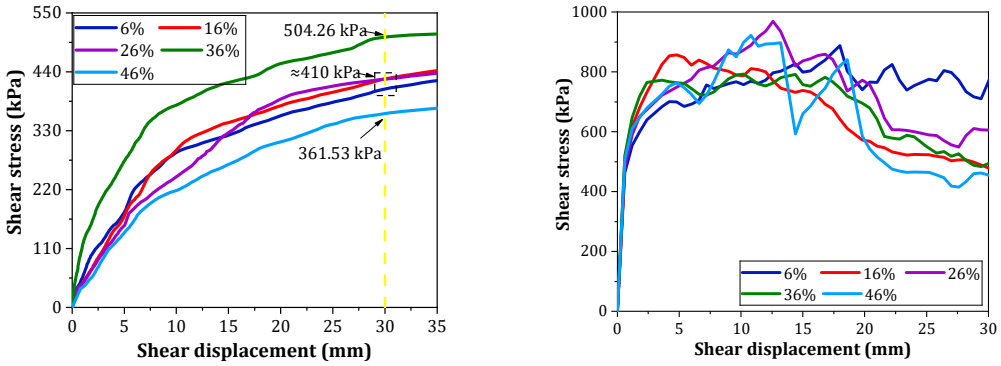

(a) Normally compacted samples (b) Fully compacted samples

Fig. 6. DEM direct shear stress-displacement curves with different contents of middle-size particles.

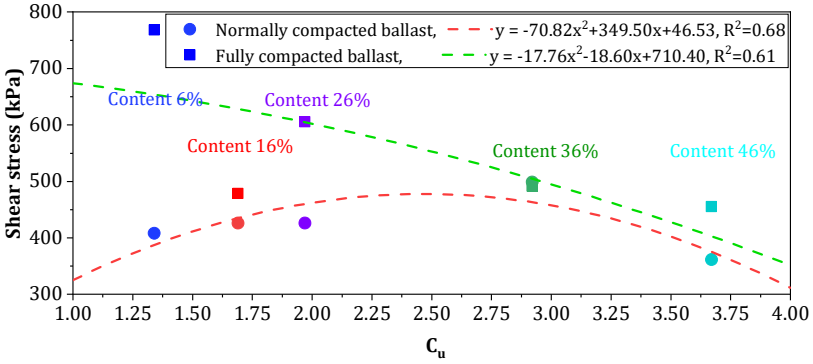

Fig. 7. C_u values and shear strengths of ballast aggregates.

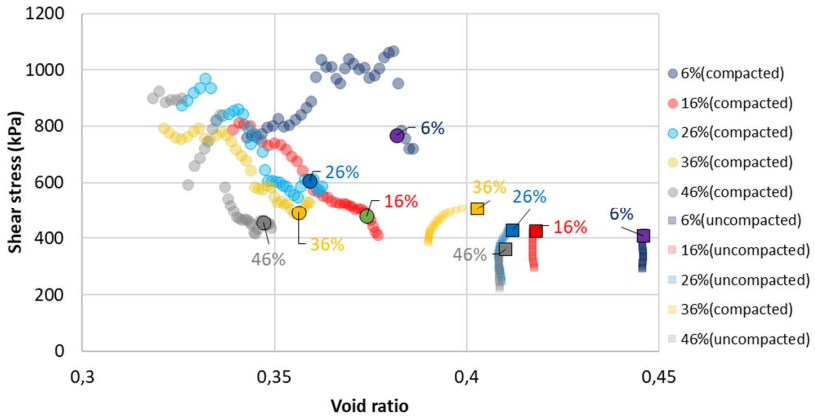

Fig. 8. Shear strengths path depending the void ratio and the points for 30 mm shear displacement.

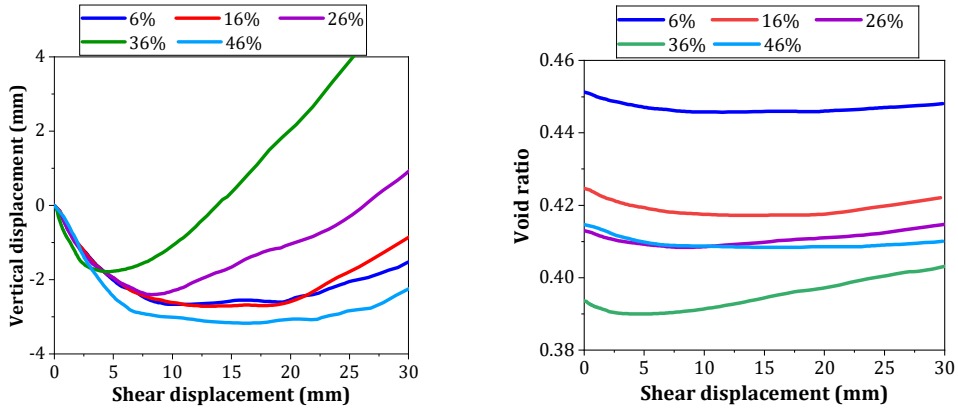

(a) Normally compacted samples

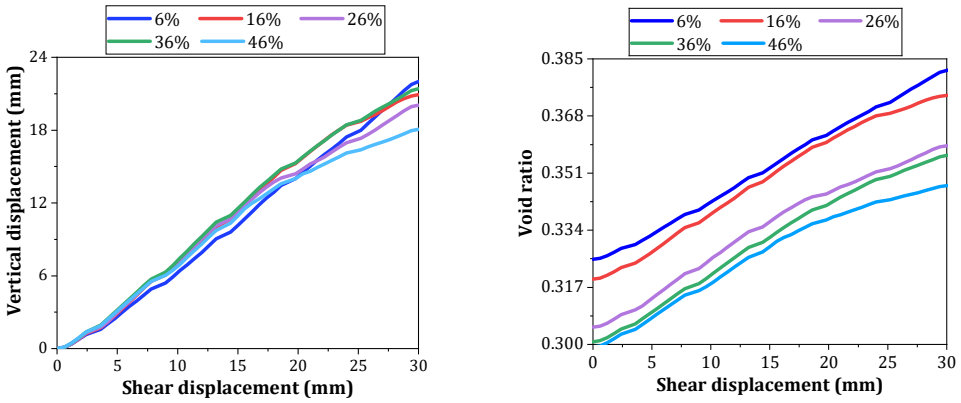

(b) Fully compacted samples

Fig. 9. Variations of vertical displacements and void ratio.

3.2.1.2 Void ratio

The bulk density and void ratio of granular materials can be converted by Equation (3). In this paper, the void ratio was used to describe the performance of the ballast aggregates. Figure 8 shows the relationship between the content of middle-size particles, void ratio and shear strength of the samples.

$$e = 1 - \frac{\rho}{\rho_a} \tag{3}$$

where e is the void ratio of materials, ρ is the bulk density, ρ_a is the solid density.

The relation of the shear stress to the void ratio for the displacements more than 10 and in the point 30mm is shown in Figure 8. The Figure 8 indicates in general the growth of the shear stress with the relative decrease of the void ration due to compaction. This is because that the decreased void ratio can provide the more contact between ballast particles [22, 23]. However, the absolute values of the void ratio for the fully compacted and normally compacted sample groups present different tendencies. The maximal shear strength of the fully compacted ballast corresponds to the samples without indention of the middle-size particles that has the highest void ratio. For the normally compacted samples the highest shear strength corresponds to the sample with the lowest void ratio.

3.2.1.3 Vertical displacement

Shear shrinkage and/or shear dilatancy occur during the direct shear tests of granular materials. This is a phenomenon due to the relative rotations and displacements of the particles in the granular aggregate during the shearing process, which increases or decreases the voids between the particles. In this section, the variation of the vertical displacements and void ratio of ballast aggregates with different contents of middle particles was recorded, as shown in Figure 9.

Figure 9 (a) shows that the five normally compacted ballast aggregates in the direct shear process had shear shrinkage in the initial stage and then shear dilatancy, and their differences are the time and magnitude of the shrinkages and dilatancy. In the initial stage, the variations of the vertical displacements with shear displacements are similar for ballast aggregates with lower contents of middle particles (Content 6%, 16%, and 26%). The state of Content 26% shifts from shear shrinkage to shear dilatancy directly when the shear displacement exceeds 8 mm. The vertical displacements of Content 6% and 16% are stable in the shear displacement range of about 8 mm to 20 mm, and they shift to shear dilatancy when their shear displacements are 20 mm. The "stable phase" also occurs for the Content 46%, except that the phase occurs earlier and lasted longer than that of Content 6% and 16%. In addition, the curves of Content 36% and 46% show more intense shear variations in their initial stages compared to the curves of Content 6%, 16% and 26%. Meanwhile, the curve of Content 36% has a faster change of shear dilatancy in the later stages, while the curve of Content 46% possesses a flat change. In addition, the five samples that were fully compacted underwent only shear dilatancy during the direct shear process. This is because their void values could no longer be reduced. Although it is obvious, it is also worth noting that the changes in the void ratio of the samples during the shear process are the same as the trends in the vertical displacements, regardless of whether the samples are normally or fully compacted.

3.2.2 Microscopic factors

The analysis in Subsection 3.2.1 showed that although the initial void ratio was an important factor affecting the shear strength of the ballast layer, the difference in the content of middle-size particles for the same initial void ratio also led to changes (shear dilatancy, shear shrinkage and shear strength) in the shear curves. Thus, this subsection analyzed the effect of middle-size particles on the direct shear properties of the ballast aggregates from a microscopic perspective using DEM simulations.

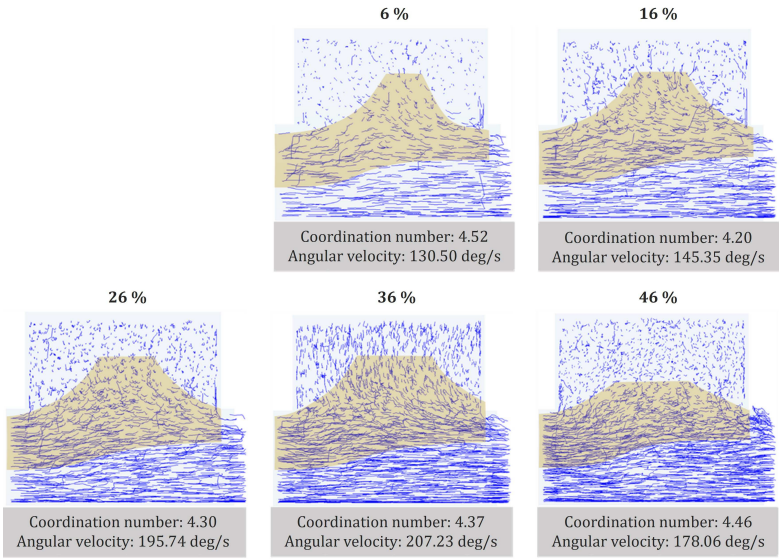

(a) Normally compacted ballast samples

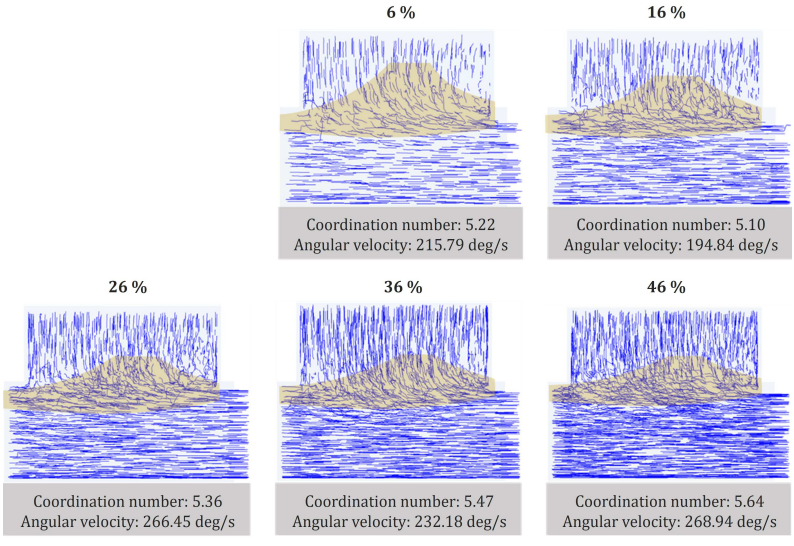

(b) Fully compacted ballast samples

Fig. 10. Movements of ballast particles and the deformation zones during the shear process.

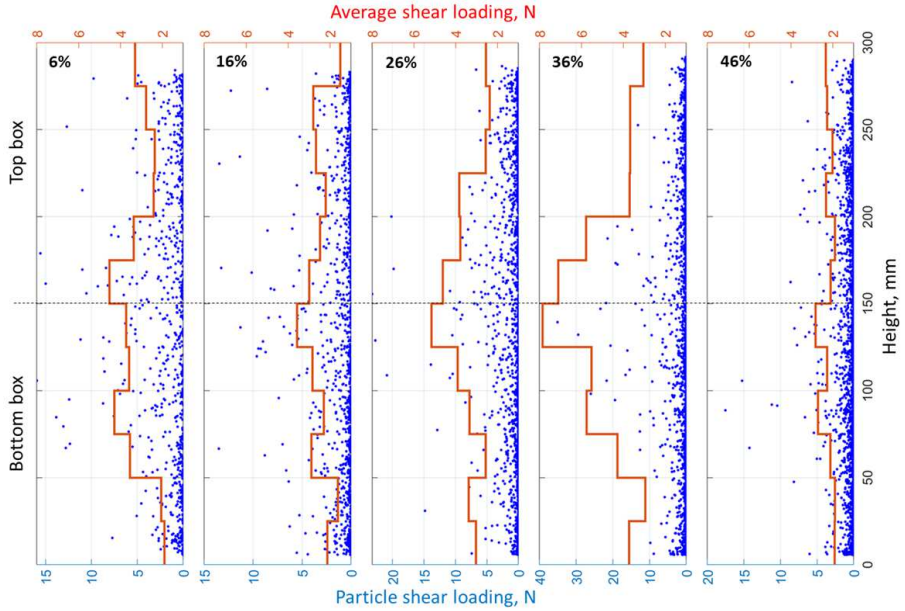

(a) Normally compacted ballast

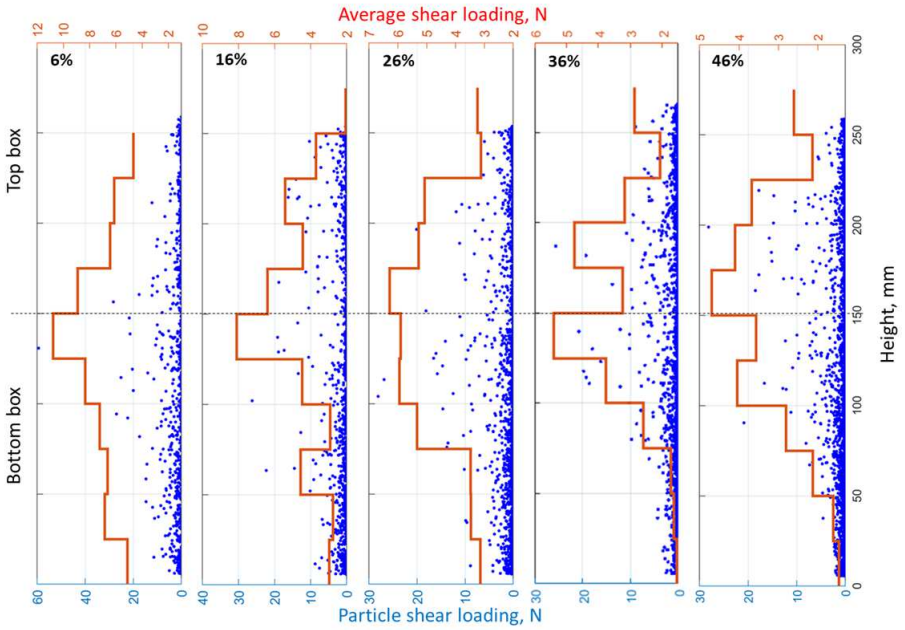

(b) Fully compacted ballast

Fig. 11. Distribution of particle shear force in the vertical direction.

3.2.2.1 Distributions and Movements of ballast particles

The above analysis has showed that the direct shear performance and the contact state of some ballast aggregates with the same void ratio are different due to the influence of middle-size particles. In order to clarify the role of middle-size particles in ballast aggregates, this subsection analyzed the distributions and movement states of particles during the direct shear process. Figure 10 shows the movements trajectories of the particles and the deformation zones. The deformation zones were selected based on the nonlinear motion of the particles.

The particle trajectories of the normally compacted ballast show that the biggest deformation zone corresponds to the content case 36%, which is also characterized with high vertical motion of the particles in the upper box. The deformation zone in the upper box for the content case 46% is more than two times lower than for the 36% case. The particles trajectories and deformation zones for the fully compacted ballast specimens present quite different relations. The trajectories for all content cases in the upper box are mostly vertical that correspond to the dilation effects, while the particles trajectories in the bottom box are mostly horizontal. The deformation zones are narrower than that of the normally compacted case. The largest deformation zone corresponds to the content case 6% and is decreasing with the growing content of middle-size particles.

3.2.2.2 Distributions and transitions of shear force

The applied shear loading is transmitted over the ballast specimens from the bottom box to the upper one. Thus, the distribution of the shear loading in the ballast is an important indicator that could explain the internal behavior of the ballast. The presentation of the shear force distributions over the vertical dimension was used based on the forces of separate particles and their averaged values of each 25mm layers (Figure 11).

The distributions of particle shear loading for the normally compacted ballast show the highest shear loading belongs to Content 36%, with the maximal loading two times higher than that of the other cases. However, the particle shear loading is very scattered over the vertical height (bule points). The averaged particles loading (red lines) show clearer that the distribution of shear loading with the maximal value of Content 36% is two times more than that of Content 6% and three times more than that of Content 46%. Additional distinctive feature of Content 36% is the vertical inhomogeneity of the shear force distribution with the maximal loading accumulation in the zone between the boxes. The particle shear loading distributions of the fully compacted ballast, different to the normally compacted cases, demonstrate the much higher shear loading which is not homogenously distributed along the vertical height. The maximal average shear loading corresponds to Content 6% and the minimal one is for Content 46%.

4. Conclusions

The presented studies in Introduction demonstrate the ballast strengthening effect of the wide range PSD more significant compared to that of the conventional narrow range PSD. Some studies proposed the alternative PSD forms. However, most studies have analyzed the problem in the narrow context without taking the additional factors (e.g., ballast compaction, ballast fragmentation etc.) as well as the reasons of the strengthening effect into account. This paper has proven theoretically, using 3D DEM simulations, the strengthening effect while adding the middle-size particles for wide range PSD in the direct shear tests for the normally compact ballast. The maximum of the strength is expected for the insertion of the 20-30% additional particles (or 26-36% overall content). The results contradict to some extent with the experimentally found in [41] 15%. However, the discrepancy between the simulations and the experiment could be explained with the different shapes of the ballast in the numerical and real tests as well as many unknown factors. The study the influence of the ballast compaction, the simulations of the shear tests in the fully compacted ballast state were present. The results show the absence of the strengthening effect after adding the middle-size particles: the maximal shear strengths were reached for the case without the additional particles (6% overall content). The insertion of the 10-40% middle-size particles cause up to double reduction of the shear strength for the shear displacement 30mm. Thus, the difference between the experimental [21] and the present simulations can be explained with higher initial compaction in the experimental study [1]. In general, it should be expected that the increase of the compaction would cause the shift of the local strength maximum from 30% to 0% of the additional particles.

The reasons of the different ballast behavior in the shear tests for the different ballast compactions can be clear observed from the macroscopic and microscopic analysis. The most evident macroscopic parameter that correlates to the local maximum of the strength is the vertical displacement: the highest strength (36% normally compacted ballast) corresponds to the maximal negative vertical displacement. The microscopic analysis show that the insertion of the additional mid-size particles causes different particle motion and the shear loading transmission. The deformation zones for the maximal strength case are the largest. However, the most evident microscopic feature of the local strength maximum is the variation of the void ratio. The normally compacted sample 36% with highest shear strengths is characterized with high dilation process while the other samples are subjected to the low contraction and the equal dilation phases. Different to it, the fully compacted samples are characterized with only dilation phase and void ratio increase that is up to five times higher than for the normally compacted samples.

In conclusion, the results show that the ballast layers with conventional narrow PSD have higher shear strength than wide range PSD if the ballast is good fully compacted. Additionally, it should be noted that the number of small particles will increase during the lifecycle of the ballast layer due to corner brakeage and the external contamination. Moreover, the drainage aspects of the wide range PSD should be considered. Thus, the excessive insertion of small and midsize particles is not justified.

It should be also noted that the circular surfaces of the particles in the DEM models cannot equivalent to the real ballast particles. Meanwhile, the physical ballast subjected to vertical pressure and horizontal shear will produce a certain amount of breakage during the direct shear tests, but the breakage of ballast particles was not considered in the DEM models. Therefore, the values in those simulations may differ from the physical experiments. In further studies, high-performance computers will be used to build more accurate ballast models in the DEM. Also, the breakage of ballast particles will be considered.

5. Expectations

Geogrid can greatly improve the stability and shear resistance of ballast layers. The main reason is that geogrid can limit the movement and rotation of ballast particles, thereby improving the contact ability and interlock ability between particles. One of our next research focuses is to explore the macroscopic and microscopic reasons for the improvement of shear performance of ballast layer by the geogrid materials through physical experiments and numerical simulations.

Author Contributions

J. Liu: Data curation, Formal analysis, Writing original and revised drafts. M. Sysyn: Conceptualization, Methodology, Supervision. Z. Liu: Investigation, Software, Resources. L. Kou: Investigation. P. Wang: Validation, Project administration. The manuscript was written through the contribution of all authors. All authors discussed the results, reviewed, and approved the final version of the manuscript.

Acknowledgments

This research was supported by the National Natural Science Foundation of China (No. U1734207) and the Fundamental Research Funds for the Central Universities (No. 2682018CX01). Thanks for the China Scholarship Council (award to Jianxing Liu (No. 202107000056) for studying abroad in the Technical University of Dresden).

Conflict of Interest

The authors declared no potential conflicts of interest concerning the research, authorship, and publication of this article.

Funding

National Natural Science Foundation of China (No. U1734207), Fundamental Research Funds for the Central Universities (No. 2682018CX01), China Scholarship Council (award to Jianxing Liu (No. 202107000056).

Data Availability Statements

The datasets generated and/or analyzed during the current study are available from the corresponding author on reasonable request.

Nomenclature

P	Percentage passing weight, $P = 100(d/D)^{0.45}$	d_{10}	Particle size whose total mass of particles is less than 10% [mm]
d	Size of aggregate [mm]	e	Void ratio of materials, $e = 1\text{-}\rho/\rho_a$
D	Maximum aggregate size [mm]	ρ	Bulk density [kg/m^3]
C_u	Coefficient of uniformity, $C_u = d_{60}/d_{10}$	ρ_a	Solid density [kg/m^3]
d_{60}	Particle size whose total mass of particles is less than 60% [mm]		

References

[1] Esveld, C., *Modern railway track*, Zaltbommel: MRT-productions, 2001.
[2] Lim, W.L., McDowell, G.R., Discrete element modelling of railway ballast, *Granular Matter*, 7(1), 2005, 19-29.
[3] Indraratna, B., Salim, W., Rujikiatkamjorn C., *Advanced rail geotechnology-ballasted track*, CRC Press, 2011.
[4] Ižvolt, L., Dobeš, P., Navikas, D., Comparison of the dimensions design methodologies of the railway track bed structure according to frost effect in Slovakia and Lithuania, *Journal of Civil Engineering and Management*, 25(7), 2019, 646-653.
[5] Tutumluer, E., Qian, Y., Hashash, Y.M., Ghaboussi, J., Davis, D.D., Discrete element modelling of ballasted track deformation behaviour, *International Journal of Rail Transportation*, 1(1-2), 2013, 57-73.
[6] Kaewunruen, S., Remennikov, A.M., Field trials for dynamic characteristics of railway track and its components using impact excitation technique, *NDT & E International*, 40(7), 2007, 510-519.
[7] Jing, G., Ding, D., Liu, X., High-speed railway ballast flight mechanism analysis and risk management–A literature review, *Construction and Building Materials*, 223, 2019, 629-642.
[8] Danesh, A., Palassi, M., Mirghasemi, A.A., Evaluating the influence of ballast degradation on its shear behavior, *International Journal of Rail Transportation*, 6(3), 2018, 145-162.
[9] Guo, Y., Markine, V., Song, J., Jing, G., Ballast degradation: Effect of particle size and shape using Los Angeles Abrasion test and image analysis, *Construction and Building Materials*, 169, 2018, 414-424.
[10] Liu, S., Huang, H., Qiu, T., Gao, Y., Study on ballast particle movement at different locations beneath crosstie using "SmartRock", *ASME/IEEE Joint Rail Conference*, American Society of Mechanical Engineers, Vol. 49675, 2016.
[11] Jing, G., Wang, J., Wang, H., Siahkouhi, M., Numerical investigation of the behavior of stone ballast mixed by steel slag in ballasted railway track, *Construction and Building Materials*, 262, 2020, 120015.
[12] Sysyn, M., Przybylowicz, M., Nabochenko, O., Kou, L., Identification of sleeper support conditions using mechanical model supported data-driven approach, *Sensors*, 21(11), 2021, 3609.
[13] Guo, Y., Jia, W., Markine, V., Jing, G., Rheology study of ballast-sleeper interaction with particle image Velocimetry (PIV) and discrete element modelling (DEM), *Construction and Building Materials*, 282, 2021, 122710.
[14] Indraratna, B., Nimbalkar, S., Christie, D., Rujikiatkamjorn, C., Vinod, J., Field assessment of the performance of a ballasted rail track with and without geosynthetics, *Journal of Geotechnical and Geoenvironmental Engineering*, 136(7), 2010, 907-917.
[15] Qian, Y., Mishra, D., Tutumluer, E., Kazmee, H.A., Characterization of geogrid reinforced ballast behavior at different levels of degradation through triaxial shear strength test and discrete element modeling, *Geotextiles and Geomembranes*, 43(5), 2015, 393-402.
[16] Dombrow, W., Huang, H., Tutumluer, E., Comparison of coal dust fouled railroad ballast behavior-granite vs. limestone, *8th International Conference on the Bearing Capacity of Roads, Railways and Airfields*, America, BCR2A'09, 2009.
[17] Wnek, M.A., Tutumluer, E., Moaveni, M., Gehringer, E., Investigation of aggregate properties influencing railroad ballast performance, *Transportation Research Record*, 2374(1), 2013, 180-189.
[18] Indraratna, B., Nimbalkar, S.S., Ngo, N.T., Neville, T., Performance improvement of rail track substructure using artificial inclusions–Experimental and numerical studies, *Transportation Geotechnics*, 8, 2016, 69-85.
[19] TolouKian, A.R., Sadeghi, J., Zakeri, J.A., Large-scale direct shear tests on sand-contaminated ballast, *Proceedings of the Institution of Civil Engineers-Geotechnical Engineering*, 171(5), 2018, 451-461.
[20] Jia, W., Markine, V., Guo, Y., Jing, G., Experimental and numerical investigations on the shear behaviour of recycled railway ballast, *Construction and Building Materials*, 217, 2019, 310-320.
[21] Stark, T.D., Swan Jr, R.H., Yuan, Z., Ballast direct shear testing, *ASME/IEEE Joint Rail Conference*, American Society of Mechanical Engineers, 2014.
[22] Estaire J., Santana M., Large direct shear tests performed with fresh ballast, *ASTM International*, 2018.
[23] Bian, X., Li, W., Qian, Y., Tutumluer, E., Micromechanical particle interactions in railway ballast through DEM simulations of direct shear tests, *International Journal of Geomechanics*, 19(5), 2019, 04019031.
[24] Alsirawan, R., Analysis of Embankment Supported by Rigid Inclusions Using Plaxis 3D, *Acta Technica Jaurinensis*, 14(4), 2021, 455-476.
[25] Habashneh, M., Special reinforcement solutions of railway permanent ways' soil substructures, *Acta Technica Jaurinensis*, 14(3), 2021, 339-363.
[26] Ahmad, M., Review of materials used for ballast reinforcement, *Acta Technica Jaurinensis*, 14(3), 2021, 315-338.
[27] Qatamin, J., Amir, I., Asphalt layers within railway tracks' substructure, *Acta Technica Jaurinensis*, 14(4), 2021, 612-631.
[28] Tigh Kuchak, A.J., Marinkovic, D., Zehn, M., Finite element model updating - Case study of a rail damper, *Structural Engineering and Mechanics*, 73(1), 2020, 27-35.
[29] Kuchak, A.J.T., Marinkovic, D., Zehn, M., Parametric Investigation of a Rail Damper Design Based on a Lab-Scaled Model, *Journal of Vibration Engineering and Technologies*, 9(1), 2021, 51-60.
[30] Indraratna, B., Khabbaz, H., Salim, W., Christie, D., Geotechnical properties of ballast and the role of geosynthetics in rail track stabilization, *Proceedings of the Institution of Civil Engineers-Ground Improvement*, 10(3), 2006, 91-101.
[31] Sysyn, M., Gerber, U., Nabochenko, O., Dehne, S., A laboratory study of pressure distribution and residual settlements in wide grading double layer railway ballast under long-term cyclic loading, *Archives of Civil Engineering*, 66(4), 2020.
[32] Fuller, W.B., Thompson, S.E., The laws of proportioning concrete, *Transactions of the American Society of Civil Engineers*, 59(2), 1907, 67-143.
[33] Roberts, F.L., Kandhal, P.S., Brown, E.R., Lee, D.Y., Kennedy, T.W., Hot mix asphalt materials, mixture design and construction, *NAPA Research and Education Foundation, Second Edition*, America, 1996.
[34] Arema, L.M.D., Manual for railway engineering, American railway engineering and maintenance-of-way association, 2019.
[35] Bian, X., Huang, H., Tutumluer, E., Gao, Y., "Critical particle size" and ballast gradation studied by discrete element modeling, *Transportation Geotechnics*, 6, 2016, 38-44.
[36] Australia, Aggregates and rock for engineering purposes (AS 2758.7): Railway ballast, Sydney, AU, 1996.
[37] Australia, Specification for supply of aggregate for ballast (TS 3402), V3.0, Rail Infrastructure Corporation, NSW, 2001.
[38] Francaise, N., Railway fix equipment: Ballast and gravel for shovel-packing (NF F53-695): Characteristics and specifications, 1996.
[39] China, TMOR. Railway Ballast (TB/T 2140-2008): Railway Industry Standard of the People's Republic of China, 2008.
[40] Germany, Technische Lieferbedingungen; Gleisschotter (DBS 918 061): Deutschen Bahn Netz AG, 2021.
[41] Profaner, H., Ein Beitrag zur Stabilisierung des Schotterbettes, *ETR – Eisenbahntechnische Rundschau*, 1(2), 1975, 52-53.
[42] Xiao, H., Zhang, Z., Cui, X., Jin, F., Experimental study and discrete element analysis of ballast bed with various sand content, *Construction and Building Materials*, 271, 2021, 121869.
[43] Cundall, P.A., A computer model for simulating progressive, large-scale movement in blocky rock system, *Proceedings of the International*

Symposium on Rock Mechanics, America, 1971.
[44] Indraratna, B., Ngo, N.T., Rujikiatkamjorn, C., Vinod, J.S., Behavior of fresh and fouled railway ballast subjected to direct shear testing: discrete element simulation, *International Journal of Geomechanics*, 14(1), 2014, 34-44.
[45] Wang, Z., Jing, G., Yu, Q., Yin, H., Analysis of ballast direct shear tests by discrete element method under different normal stress, *Measurement*, 63, 2015, 17-24.
[46] TolouKian, A.R., Sadeghi, J., Zakeri, J.A., Large-scale direct shear tests on sand-contaminated ballast, *Proceedings of the Institution of Civil Engineers-Geotechnical Engineering*, 171(5), 2018, 451-461.
[47] Qian, Y., Mishra, D., Tutumluer, E., Hashash, Y.M., Ghaboussi, J., Moisture effects on degraded ballast shear strength behavior, *ASME/IEEE Joint Rail Conference*, American Society of Mechanical Engineers, Vol. 49675, 2016.
[48] Fischer, S., Breakage test of railway ballast materials with new laboratory method, *Periodica Polytechnica Civil Engineering*, 61(4), 2017, 794-802.
[49] Suhr, B., Marschnig, S., Six, K., Comparison of two different types of railway ballast in compression and direct shear tests: experimental results and DEM model validation, *Granular Matter*, 20(4), 2018, 1-13.
[50] Juhasz, E., Fischer, S., Specific evaluation methodology of railway ballast particles' degradation, *Science and Transport Progress*, 3(81), 2019, 96-109.
[51] Danesh, A., Palassi, M., Mirghasemi, A.A., Effect of sand and clay fouling on the shear strength of railway ballast for different ballast gradations, *Granular Matter*, 20(3), 2018, 1-14.

ORCID iD

Jianxing Liu https://orcid.org/0000-0002-4779-7761
Mykola Sysyn https://orcid.org/0000-0001-6893-0018
Zhiye Liu https://orcid.org/0000-0003-4394-3802
Lei Kou https://orcid.org/0000-0001-5372-6305
Ping Wang https://orcid.org/0000-0002-2088-9279

How to cite this article: Liu J., Sysyn M., Liu Z., Kou L., Wang P. Studying the Strengthening Effect of Railway Ballast in the Direct Shear Test due to Insertion of Middle-size Ballast Particles, *J. Appl. Comput. Mech.*, 8(4), 2022, 1387–1397. https://doi.org/10.22055/jacm.2022.40206.3537